

Adaptive GPS/INS integration for relative navigation

Je Young Lee · Hee Sung Kim · Kwang Ho Choi ·
Joonhoo Lim · Sebum Chun · Hyung Keun Lee

Received: 4 March 2014 / Accepted: 12 February 2015 / Published online: 4 March 2015
© Springer-Verlag Berlin Heidelberg 2015

Abstract Relative navigation based on GPS receivers and inertial measurement units is required in many applications including formation flying, collision avoidance, cooperative positioning, and accident monitoring. Since sensors are mounted on different vehicles which are moving independently, sensor errors are more variable in relative navigation than in single-vehicle navigation due to different vehicle dynamics and signal environments. In order to improve the robustness against sensor error variability in relative navigation, we present an efficient adaptive GPS/INS integration method. In the proposed method, the covariances of GPS and inertial measurements are estimated separately by the innovations of two fundamentally different filters. One is the position-domain carrier-smoothed-code filter and the other is the velocity-aided Kalman filter. By the proposed two-filter adaptive estimation method, the covariance estimation of the two sensors can be isolated effectively since each filter estimates its own measurement noise. Simulation and experimental results demonstrate that the proposed method improves relative navigation accuracy by appropriate noise covariance estimation.

Keywords GPS/INS integration · Relative navigation · Adaptive estimation · CSC filtering

J. Y. Lee · H. S. Kim · K. H. Choi · J. Lim · H. K. Lee (✉)
School of Electronics, Telecommunication and Computer
Engineering, Korea Aerospace University, 100, Hanggongdae
gil, Hwajeon-dong, Deogyang-gu, Goyang-City,
Gyeonggi-do 412-791, Korea
e-mail: hyknlee@kau.ac.kr

S. Chun
Satellites Navigation Team, CNS/ATM and Satellite Navigation
Research Center, Korea Aerospace Research Institute, 169-84
Gwahak-ro, Yuseong-gu, Daejeon 305-806, Korea

Introduction

Relative navigation is purposed to provide relative position, velocity, and attitude between separately moving vehicles accurately and reliably. It enables highly complex missions such as formation flying, vehicle-to-vehicle collision avoidance, cooperative positioning, and accident monitoring. In addition, combined with the recently introduced networked vehicles based on wireless communication, it can produce many innovative applications in the near future (Dar et al. 2010; Gerla and Kleinrock 2011).

As in the case of conventional single-vehicle navigation, the integration of the global positioning system (GPS) and the inertial navigation system (INS) is one of the most effective ways for relative navigation between multiple vehicles (Yun et al. 1999; Fosbury and Crassidis 2006). The most representative GPS/INS integration methods are the loosely coupled (LC) and tightly coupled (TC) methods. Among the two methods, the LC method is advantageous regarding implementation simplicity but bears theoretically undesirable problems since two filters are arranged in cascaded form (Groves 2008; Kaplan and Hegarty 2006). The TC method offers theoretical soundness but imposes heavy computational burden since a large number of system states need to be considered by a single integration filter.

Related to the mechanization of relative navigation, several notable methods were introduced recently. Alonso et al. (2000) proposed a method utilizing multiple line of sight (LOS) vectors to estimate the relative position and velocity between multiple satellites in formation. Bever et al. (2002) compared the characteristics of three relative navigation approaches; independent separation measurement system, formation needles, and formation flight instrumentation system.

Since many sensors are used in relative navigation, time synchronization is very important. Related to the time synchronization in multi-sensor fusion, an analytic calibration method was proposed by Lee et al. (2002), a GPS-slaved time synchronization method was introduced by Li et al. (2006), a method using a counter and two latching registers was employed by Ding et al. (2008), and a method to estimate the constant time synchronization error by time stamp filtering was proposed by Nilsson and Handel (2010).

Since sensors are mounted on different vehicles moving independently, sensor errors are more variable in relative navigation than in conventional single-vehicle navigation due to different vehicle dynamics and signal environments. For the reason, a critical factor for the accuracy improvement is the treatment of variable error characteristics. To resolve this problem, adaptive estimation methods have been used traditionally to improve estimation accuracy in the presence of time-varying errors (Magill 1965; Mehra 1970, 1971). In adaptive filtering, time-varying process and measurement error covariances are estimated based on residual vectors. The most representative methods in this category are the multiple-model-based adaptive estimation (MMAE) method and the innovation-based adaptive estimation (IAE) method (Mohamed and Schwarz 1999).

In MMAE, a bank of local filters with different statistical models runs simultaneously (Maybeck 1989; Hanlon and Maybeck 2000). The overall system states are estimated by combining all the local filters. MMAE imposes heavy computational burden due to the utilization of many filters at the same time. In IAE, the noise covariance matrices are estimated sequentially based on innovation vectors (Kailath 1971; Mehra 1970, 1971). Since IAE utilizes a single filter, it can reduce computational burden as compared with MMAE.

Related to navigation, adaptive estimation methods were applied to attitude and heading reference systems (AHRS) (Li and Wang 2013), GPS/INS integration (Hao et al. 2009; Zhou et al. 2010; Fakharian et al. 2011), and velocity estimation (Chu et al. 2010). Ding et al. (2007) investigated an online stochastic modeling algorithm and proposed a new adaptive scaling algorithm. Almagbile et al. (2010) compared the innovation and residual vectors in adaptive estimation.

Recently, studies on adaptive relative navigation have been published. Li et al. (2013) proposed an adaptive robust Kalman filter (KF) derived for both process and measurement noise uncertainties. This method improves the robustness of the methodology proposed by Garcia-Velo (1997) and can be implemented in GPS-based relative navigation with orbit perturbations and non-Gaussian random measurement errors. Baek and Bang (2013) proposed an adaptive sparse-grid quadrature filter for spacecraft's

relative navigation. This method adjusts the accuracy level of the filter autonomously with a quadrature error adaptation criterion.

To improve the robustness against sensor error variability in relative navigation, we propose an efficient adaptive GPS/INS integration method. Compared with conventional methods, the proposed method estimates the covariances of GPS and inertial measurements separately by the innovations of two fundamentally different filters. One is the position-domain carrier-smoothed-code filter and the other is the velocity-aided KF. By the proposed two-filter adaptive estimation method, covariance estimation procedures for GPS measurement noise and inertial propagation noise can be isolated effectively since each filter estimates its own measurement noise.

First, the relative inertial navigation algorithm is explained and the overall two-filter architecture for GPS/INS integration is introduced. Next, an adaptive position-domain carrier-smoothed-code filter (CSCF) and an adaptive KF are explained. The adaptive CSCF is used for relative positioning and the adaptive KF is used to obtain relative velocity and attitude for improved accuracy. The last section deals with simulation and experiment results to demonstrate the feasibility of the proposed method. Finally, concluding remarks will be given.

Relative inertial navigation algorithm

Figure 1 shows the configuration of different frames used in this research. The inertial-frame (i-frame) is a reference frame in which Newton's laws of motion apply with non-accelerating but possibly uniform linear motion. The earth-centered, earth-fixed (ECEF) frame (e-frame) is fixed to the center of the earth. The x -axis intersects 0 degree latitude and 0 degree longitude, the z -axis is pointing toward the north, and the y -axis follows the right-handed rule. The navigation-frame (n-frame) is aligned to the local north,

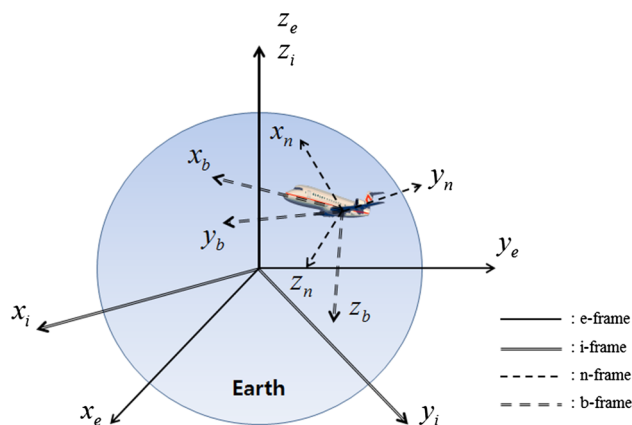


Fig. 1 Configuration of different frames

east, and downward directions. The body-frame (b-frame) is fixed to the center of gravity of the vehicle and aligned to the vehicle’s forward, right, and downward directions. In relative navigation, the master and slave vehicles correspond to different body frames. To discriminate the body frames related to different vehicles, the master frame (m-frame) and the slave frame (s-frame) are utilized.

To obtain high rate relative velocity and attitude, relative angular velocity and specific force are formed by differencing between the master and slave vehicles,

$$\omega_{rel} = \omega_{is}^s - C_m^s \omega_{im}^m \tag{1}$$

$$f_{rel} = f^s - C_m^s f^m \tag{2}$$

where f indicates the specific force, ω_{is} indicates the angular rate of s-frame from i-frame, C_m^s indicates the transformation matrix from m-frame to s-frame, respectively. Based on the inertial velocity and attitude equations (Lee et al. 1998), relative velocity and attitude are computed as follows,

$$\dot{V}_{rel} = C_s^n f_{rel} - (2\Omega + \rho) \times V_{rel} \tag{3}$$

$$\dot{Q}_{rel} = \frac{1}{2} U(Q_{rel}) \omega_{rel} \tag{4}$$

$$Q_{rel} = [q_0 \quad q_1 \quad q_2 \quad q_3]^T \tag{5}$$

$$U(Q_{rel}) = \begin{bmatrix} -q_1 & -q_2 & -q_3 \\ q_0 & -q_3 & q_2 \\ q_3 & q_0 & -q_1 \\ -q_2 & q_1 & q_0 \end{bmatrix} \tag{6}$$

where V_{rel} indicates the relative velocity expressed in n-frame, Ω indicates the earth rate expressed in the n-frame, ρ indicates the transport rate expressed in n-frame, and Q_{rel} indicates the relative quaternion representing the rotation from m-frame to s-frame.

It is assumed in (3) that the master and slave vehicles are under practically the same local gravity field since they are located closely. By applying the similar procedure outlined in Lee et al. (1998), the error dynamics model for relative navigation can be derived as follows,

$$\dot{X} = FX + GW \tag{7}$$

$$X = [X_{INS}(s)^T \quad \delta r_{LAE}(s)^T \quad \delta t_{SE}(s)]^T \tag{8}$$

$$X_{INS}(s)^T = [\delta V_{rel} \quad \psi_{rel} \quad \nabla_s \quad \varepsilon_s] \tag{9}$$

$$W = [w_{rela}^T \quad w_{relg}^T]^T \tag{10}$$

$$F = \begin{bmatrix} F_{11} & F_{12} & O_{6 \times 4} \\ O_{6 \times 6} & O_{6 \times 6} & O_{6 \times 4} \\ O_{4 \times 6} & O_{4 \times 6} & F_{33} \end{bmatrix} \tag{11}$$

$$F_{11} = \begin{bmatrix} -(2\omega_{ie}^n + \omega_{en}^n) \times & (C_s^n f_{rel}) \times \\ O_{3 \times 3} & -(\omega_{in}^n) \times \end{bmatrix} \tag{12}$$

$$F_{12} = \begin{bmatrix} C_s^n & O_{3 \times 3} \\ O_{3 \times 3} & -C_s^n \end{bmatrix} \tag{13}$$

$$F_{33} = \begin{bmatrix} O_{3 \times 3} & O_{3 \times 1} \\ O_{1 \times 3} & -1/\tau \end{bmatrix} \tag{14}$$

$$G = \begin{bmatrix} C_s^n & O_{3 \times 3} \\ O_{3 \times 3} & -C_s^n \\ O_{10 \times 3} & O_{10 \times 3} \end{bmatrix} \tag{15}$$

where δr_{LAE}^T is the relative lever arm error expressed in the n-frame, δt_{SE}^T is the time synchronizing error between GPS and inertial measurements, δV_{rel} is the relative velocity error expressed in the n-frame, ψ_{rel} is the relative attitude error expressed in m-frame, ∇_s is the relative accelerometer bias expressed in s-frame, ε_s is the relative gyro drift expressed in s-frame, w_{rela} is the relative accelerometer white noise expressed in s-frame, and w_{relg} is the relative gyro white noise expressed in s-frame.

It is assumed in (7) that the inertial sensor biases ∇_m and ε_m of the master INS are negligibly small compared to inertial sensor biases ∇_s and ε_s of the slave INS due to self-compensation of the master INS, pre-filtering with a stand-alone algorithm, or utilizing a higher-grade IMU for the master vehicle. To obtain feasible accuracy with minimum hardware, both the lever arm errors and the time synchronization error between GPS and INS are also considered as shown in (8).

Configuration of relative GPS/INS integration

For GPS/INS integration, the LC and TC methods have been widely utilized. Among the two representative methods, the LC method is advantageous in terms of implementation simplicity. However, in the LC method, the output of a GPS filter may be used as the input to the integration KF. In this case, the errors in GPS position solutions used in the KF measurement updates are not white but temporally correlated. For this reason, cascaded filtering problem may occur in the LC method (Groves 2008; Kaplan and Hegarty 2006). In this case, the basic KF assumption is not satisfied since the KF assumes that measurement and process errors are white Gaussian for theoretical optimality. Even when snapshot methods are utilized in computing position solutions, temporally correlated error also appears due to the ionospheric and tropospheric errors.

In comparison with the LC method, the TC integration utilizes raw GPS measurements. Due to the utilization of raw measurements, the cascaded filtering problem can be avoided. However, when the number of visible GPS satellites increases, the total number of filter states

increases considerably. The increased number of states may cause a significant computational burden.

To combine the advantages and avoid the disadvantages of the traditional LC and TC methods, a two-filter GPS/INS integration method was proposed recently (Park et al. 2011). The configuration of the GPS/INS integration based on the two filters is shown in Fig. 2. The figure shows that the CSCF estimates accurate position and the KF estimates the remaining INS error states. The CSCF is advantageous in obtaining relative positions with centimeter-level accuracy, and the KF can provide high-speed velocity and attitude outputs. The high-speed relative positions can be obtained by combining the CSCF-provided position and the KF-provided velocity. It should be noted that, since the KF utilizes accurate GPS velocity formed by carrier phase measurements instead of a pre-filter, the cascaded filtering problem does not occur in the proposed method since raw measurements are utilized as the input to each filter.

Extending the previous two-filter method, the proposed adaptive GPS/INS integration method also implements two heterogeneous filters, the adaptive single differencing (SD) position-domain (PD) CSCF and the adaptive GPS/INS KF. The architecture of the proposed adaptive method is shown in Fig. 3, where the adaptive SD PD CSCF is applied to the GPS measurements and the adaptive GPS/INS KF is applied to the relative INS.

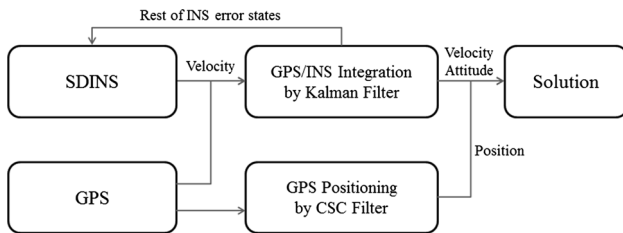


Fig. 2 Configuration of GPS/INS integration based on two filters

the relative inertial measurements are utilized as input to the relative INS algorithm to obtain the relative attitude and velocity at high output rate. GPS measurements are utilized as input to the adaptive SD PD CSCF for relative positioning. Also, GPS carrier phase measurements are utilized to compute the GPS relative velocity. Finally, the relative velocities and estimated noise covariance are utilized as the input to the adaptive KF for accurate relative velocity and attitude.

Adaptive estimation methods

In order to improve accuracy by estimating noise covariances, two filters are proposed, an adaptive single differencing position-domain CSCF and an adaptive GPS/INS KF. They utilize innovation sequences representing differences between estimated and actual measurements. The noise covariances of GPS measurements are estimated by the adaptive CSCF, and the noise covariances of inertial measurements are estimated by the adaptive KF.

Adaptive single differencing position-domain CSCF

The CSC filtering approach was proposed by Hatch (1983) for high-accuracy GPS applications. Compared with Kalman filtering, CSC filtering does not require any dynamics model for the time propagation of system states. Instead, it utilizes high-accuracy carrier phase measurements to account for the incremental positions between two successive time instants. Since the CSCF does not utilize any dynamics model, the carrier phase measurement noise becomes the main error source for time propagations. For the reason, accurate time propagation in CSC filtering requires accurate covariance estimation of carrier phase measurements. Related to this problem, the adaptive double

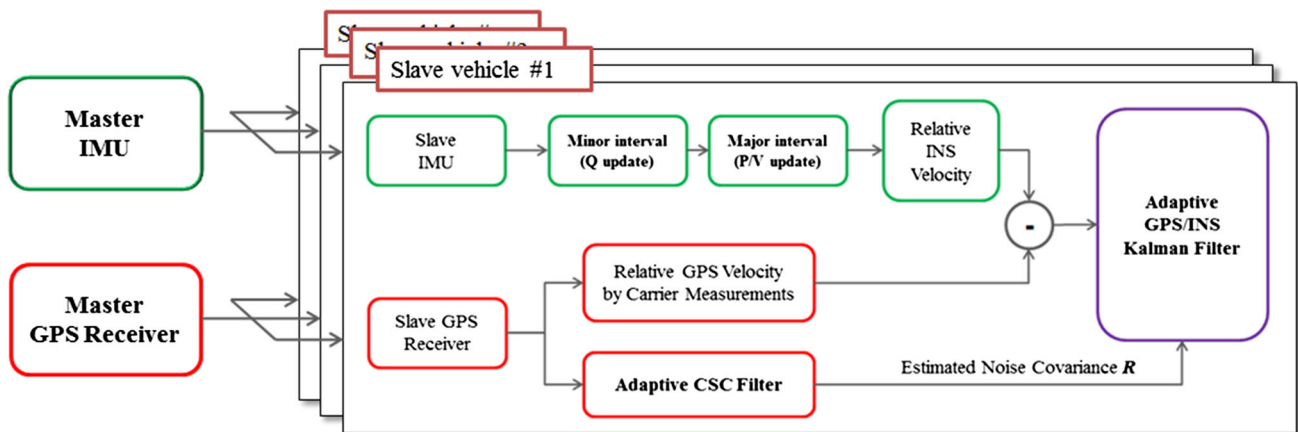


Fig. 3 Configuration of proposed relative GPS/INS Integration

Table 1 PD CSC filter algorithm

	Summary of equations
Time propagation	$H_k^* = \Gamma_k H_k, H_{k-1}^s = \Gamma_k H_{k-1}, \Omega_k^* = \Gamma_k \Omega_k$ $U_k^* = \left[(H_k^*)^T H_k^* \right]^{-1} (H_k^*)^T$ $\bar{X}_k = \hat{X}_{k-1} + U_k^* \Omega_k^*$ $\bar{P}_k = U_k^* \begin{bmatrix} H_{k-1}^s \hat{P}_{k-1} (H_{k-1}^s)^T - 2r_\phi I \\ -r_\phi H_{k-1}^s (I - K_{k-1}^* H_{k-1}^*) U_{k-1}^* \Gamma_{k-1} \Gamma_k^T \\ -r_\phi \Gamma_k \Gamma_{k-1}^T (U_{k-1}^*)^T (I - K_{k-1}^* H_{k-1}^*)^T (H_{k-1}^s)^T \end{bmatrix} (U_k^*)^T$
Measurement update	$K_k^* = \left\{ \bar{P}_k - r_\phi \left[(H_k^*)^T H_k^* \right]^{-1} \right\} (H_k^*)^T \left[H_k^* \bar{P}_k (H_k^*)^T + r_p I \right]^{-1}$ $Z_k^* = \Gamma_k Z_k$ $\hat{X}_k^* = \bar{X}_k - K_k^* Z_k^*$ $\hat{P}_k = (I - K_k^* H_k^*) \bar{P}_k (I - K_k^* H_k^*)^T + r_p K_k^* (K_k^*)^T$

differencing (DD) PD CSCF was recently proposed (Lee et al. 2011). However, since the structure of DD measurements causes additional computational complexity due to the concept of reference satellite, the DD form is not suitable for relative navigation. For the reason, we focus on the adaptive SD PD CSCF.

A representative algorithm of the PD CSCF is summarized in Table 1. More details on the PD CSC principle can be found in Lee and Rizos (2008) and Lee et al. (2005). The variables utilized in Table 1 are summarized as follows,

$$X_k = \begin{bmatrix} x_{u,k} \\ b_{u,k} \end{bmatrix}, H_k = [h_{1,k} \quad h_{2,k} \quad \cdots \quad h_{j,k}]^T \tag{16}$$

$$Z_k = H_k \delta \bar{X}_k + \varepsilon_{p,k} \tag{17}$$

$$\Omega_k = H_k \Delta X_{k-1} + W_k \tag{18}$$

$$W_k = -\Delta H_{k-1} \delta \hat{X}_{k-1} - \varepsilon_{\phi,k} + \varepsilon_{\phi,k-1} \tag{19}$$

$$\Delta X_{k-1} = X_k - X_{k-1} \tag{20}$$

$$\delta \bar{X}_{k-1} = \bar{X}_{k-1} - X_{k-1}, \quad \delta \hat{X}_{k-1} = \hat{X}_{k-1} - X_{k-1} \tag{21}$$

$$\Delta H_{k-1} = H_k - H_{k-1}, \quad h_{j,k} = [e_{j,k}^T \quad -1]^T \tag{22}$$

where \tilde{p}_k and $\tilde{\phi}_k$ are the pseudorange and carrier phase measurements, respectively, H_k is the observation matrix, $e_{j,k}$ is the difference of LOS vector between the reference and the j -th satellites, k is the time index, j is the satellite index, \bar{X}_k is a priori relative position estimate, \hat{X}_k is a posteriori relative position estimate, $\delta \bar{X}_k$ is a priori relative position error, $\delta \hat{X}_k$ is a posteriori relative position error, ΔX_k is the relative position increment, \bar{P}_k is a priori relative position error covariance, \hat{P}_k is a posteriori relative position error covariance, r_p and r_ϕ are the noise of pseudorange and carrier phase measurements, respectively, $\varepsilon_{p,k}$ and $\varepsilon_{\phi,k}$ are pseudorange and carrier phase measurement noise, respectively, and Γ_k is the satellite channel selection matrix with elements of 0 and 1.

In PD CSC filtering, the dimension of the measurement vector changes from time to time depending on the number of visible satellites. The estimate $\Delta \hat{X}_k$ can be obtained based on the carrier phase measurement vector Π_{k+1} for time propagation as follows,

$$\begin{aligned} \Delta \hat{X}_{k-1} &= H_k^+ \Pi_k \\ &= \Delta X_{k-1} - H_k^+ \Delta H_{k-1}^+ \delta \hat{X}_{k-1} + H_k^+ (N_k - N_{k-1}) \end{aligned} \tag{23}$$

$$H_k^+ = (H_k^T H_k)^{-1} H_k^T \tag{24}$$

where N_k is the carrier phase measurement noise vector. The innovation sequence $Z_{\phi,k}$ can be obtained by differencing the indirect measurement Π_k and the estimated value $H_k \Delta \hat{X}_{k-1}$ as follows,

$$\begin{aligned} Z_{\phi,k} &= \Pi_k - H_k \Delta \hat{X}_{k-1} \\ &= (I - H_k H_k^+) (N_k - N_{k-1}) - (I - H_k H_k^+) \Delta H_{k-1} \delta \hat{X}_{k-1} \end{aligned} \tag{25}$$

Based on (25), the covariance of the innovation vector can be modeled by

$$\begin{aligned} E \{ Z_{\phi,k} Z_{\phi,k}^T \} &= (I - H_k H_k^+) R_{\phi,k} (I - H_k H_k^+)^T \\ &\quad + (I - H_k H_k^+) \Delta H_{k-1} \hat{P}_{k-1} \Delta H_{k-1}^T (I - H_k H_k^+)^T \end{aligned} \tag{26}$$

$$R_{\phi,k} = E \{ (N_k - N_{k-1})(N_k - N_{k-1})^T \} \tag{27}$$

$$\hat{P}_{k-1} = E \{ \delta \hat{X}_{k-1} \delta \hat{X}_{k-1}^T \} \tag{28}$$

For further simplification, it is assumed that the following approximation is valid between two successive time instants. This assumption can be justified since the observation matrix consists of LOS vectors which are making nearly two revolutions (6.28 rad) each day based on the orbital characteristics of the navigation satellites.

The assumption is modeled by the following approximation,

$$(I - H_k H_k^+) \Delta H_{k-1} \hat{P}_{k-1} \Delta H_{k-1}^T (I - H_k H_k^+)^T \cong O \quad (29)$$

where O represents the zero matrix of appropriate dimension. It should be noted that (29) is easily satisfied in most cases when GPS measurements are sampled at higher than 1 Hz. With this assumption, the estimated carrier phase noise covariance $\hat{R}_{\phi,k}$ can be modeled as,

$$\hat{R}_{\phi,k} = E \left\{ Z_{\phi,k} Z_{\phi,k}^T \right\} \left\{ (I - H_k H_k^+) (I - H_k H_k^+)^T \right\}^{-1} \quad (30)$$

In order to estimate the pseudorange noise covariance, the proposed method computes the innovation sequence similar to the case of carrier phase measurements. The pseudorange noise covariance is required in measurement updates. The innovation sequence $Z_{p,k}$ can be obtained as follows before each measurement update,

$$Z_{p,k} = H_k \bar{X}_k - Y_k \quad (31)$$

where Y_k indicates the real pseudorange measurements. Similar to (26), the instantaneous covariance matrix of the innovation vector can be modeled by

$$\bar{M}_{p,k} = E \left\{ Z_{p,k} Z_{p,k}^T \right\} \quad (32)$$

For more reliability, the smoothed covariance matrix $\hat{M}_{p,k}$ can be obtained by averaging within the pre-defined time interval as follows,

$$\hat{M}_{p,k} = E \{ \bar{M}_p \} = \frac{1}{B} \sum_{j=k-B+1}^k \bar{M}_{p,j} \quad (33)$$

where B indicates the pre-defined averaging interval. Finally, the covariance matrix of pseudorange measurement error is obtained by

$$\hat{R}_{p,k} = \hat{M}_{p,k} - H_k \bar{P}_k H_k^T \quad (34)$$

The proposed adaptive CSCF estimates the noise covariance utilizing actual carrier phase and pseudorange measurements as shown in (30) and (34). Consequently, the adaptive CSCF takes the role of accurate position estimation with estimated measurement noise and provides the noise covariance matrices of pseudorange and carrier phase measurements.

Adaptive GPS/INS KF

In the proposed method, the adaptive velocity-aided GPS/INS KF is closely interlaced with the adaptive CSCF. As explained in the previous section, the carrier phase noise covariance is already estimated by the innovation sequences obtained by CSCF. Thus, for the measurement updates of

KF, the previously obtained carrier phase noise can be utilized. This procedure reduces computational burden of the adaptive KF by removing unnecessary covariance estimation for carrier phase measurements. Figure 4 shows the architecture of the proposed adaptive GPS/INS KF.

At each KF measurement update, the previously estimated covariances $\hat{R}_{\phi,k-1}$ and $\hat{R}_{\phi,k}$ assist in computing the covariance $\hat{R}_{A_{GPS}}$ of the relative velocity measurement A_{GPS}^n as follows,

$$\begin{aligned} \hat{R}_{A_{GPS}} &= E [\delta A_{GPS}^n \delta A_{GPS}^{nT}] \\ &= C_e^n H_k^+ \hat{R}_{\phi,k} H_k^{+T} C_e^{nT} + C_e^n H_{k-1}^+ \hat{R}_{\phi,k-1} H_{k-1}^{+T} C_e^{nT} \end{aligned} \quad (35)$$

$$A_{GPS}^n = C_e^n H_k^+ Y_k - C_e^n H_{k-1}^+ Y_{k-1} \quad (36)$$

where Y_{k-1} and Y_k indicate the relative carrier phase measurements at the previous and current time instants, respectively. As shown in (36), the covariance is affected by the carrier phase noise covariance. Since the carrier phase noise covariance is already computed by the adaptive CSCF as shown in (30), the measurement noise covariance can be obtained without additional complicated computations.

Before the KF measurement update, the indirect measurement considering lever arm compensation is formed as follows,

$$\begin{aligned} Z_k &= H \bar{X}_k - A_{GPS}^n \\ &= A_{INS}^n + \left(I_{3 \times 3} - \langle \hat{\Psi}_{bl}^n \rangle \right) C_{bl}^n \langle \hat{\omega}_{im}^m \rangle \hat{r}^m \\ &\quad - \left(I_{3 \times 3} - \langle \hat{\Psi}_s^n \rangle \right) C_s^n \langle \hat{\omega}_{is}^s \rangle \hat{r}^s - A_{GPS}^n \end{aligned} \quad (37)$$

where $\langle x \rangle$ indicates the 3×3 skew-symmetric matrix constructed by the 3×1 vector x , Ψ^n indicates the attitude error, and \hat{r} indicates the lever arm vector. The a priori INS error state \bar{X}_k and its covariance matrix \bar{P}_k for the current measurement update are obtained by the following equations,

$$\bar{X}_k = \Phi_k \hat{X}_{k-1} \quad (38)$$

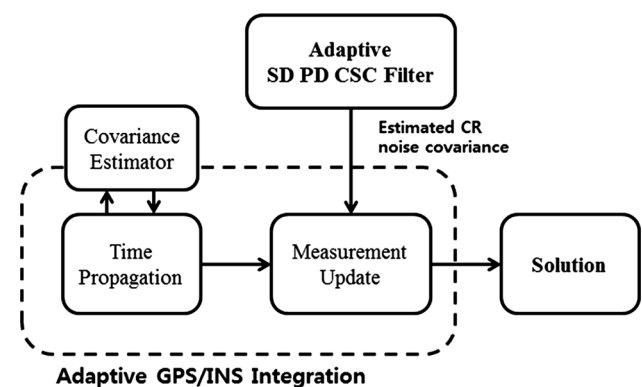


Fig. 4 Architecture of Adaptive GPS/INS Kalman filter

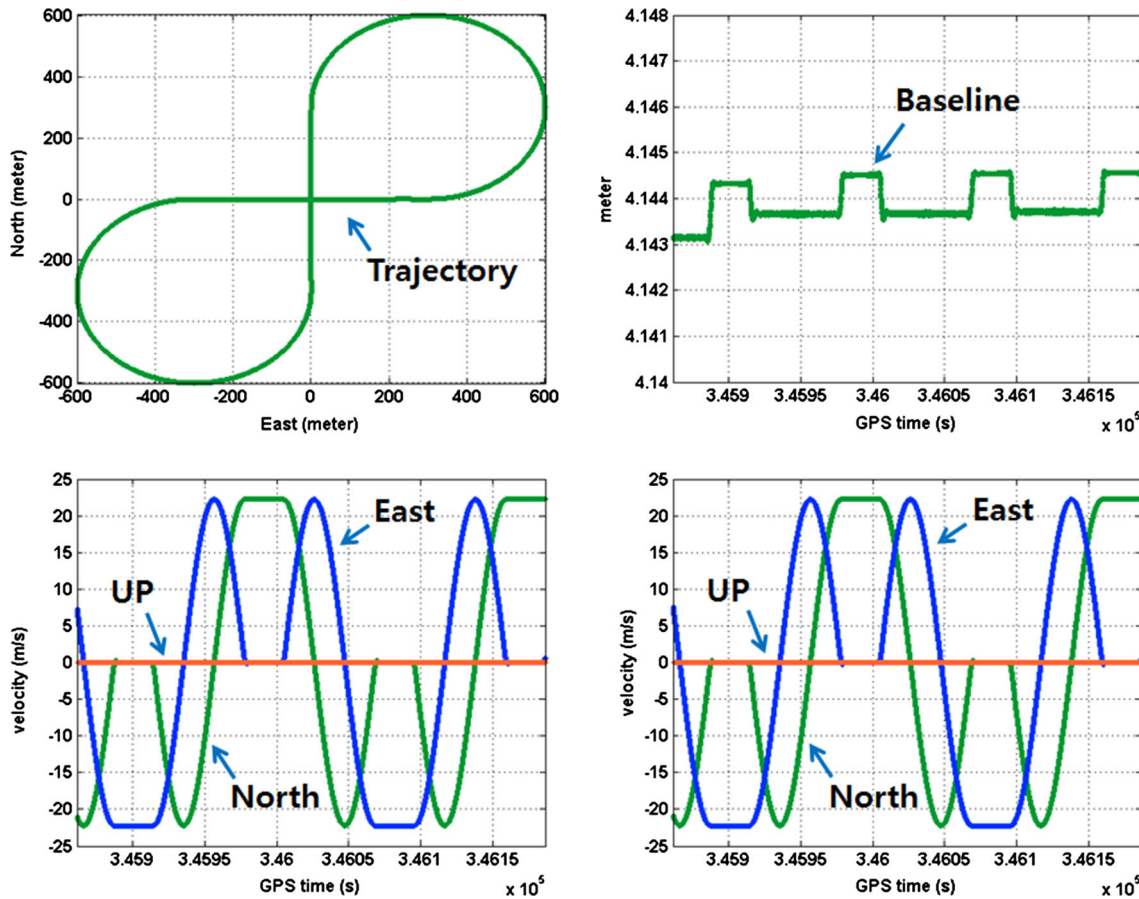


Fig. 5 Trajectory, baseline, and relative velocity of simulation

$$\bar{P}_k = \Phi_k \hat{P}_{k-1} \Phi_k^T + \hat{Q}_k \tag{39}$$

$$\Phi_k = I + F(t_k)\Delta t + \frac{F^2(t_k)\Delta t^2}{2} \tag{40}$$

where t_k indicates the k -th time instant, Δt indicates the time interval between t_{k-1} and t_k , and F can be found in (11). \hat{X}_{k-1} and \hat{P}_{k-1} appearing in (38) and (39) indicate a posteriori INS error state and its covariance matrix after the previous measurement update. The observation matrix for the measurement update can be derived as follows.

$$H = [I \quad C_s^n \langle C_m \langle \hat{\omega}_{im}^m \rangle \hat{r}^m \rangle \quad 0_{3 \times 3} \quad C_{b2}^n \langle \hat{r}^s \rangle \quad -C_{b2}^n \langle \hat{\omega}_{is}^s \rangle \quad \hat{A}^n] \tag{41}$$

Finally, the measurement update is performed by the following equations,

$$K_k = \bar{P}_k H_k^T [H_k \bar{P}_k H_k^T + \hat{R}_{AGPS}]^{-1} \tag{42}$$

$$\hat{P}_k = [I - K_k H_k] \bar{P}_k [I - K_k H_k]^T + K_k \hat{R}_{AGPS} K_k^T \tag{43}$$

$$\hat{X}_k^+ = K_k Z_k \tag{44}$$

where K_k indicates the Kalman gain. After the measurement update, the instantaneous innovation covariance

matrix \bar{M}_k and the smoothed innovation covariance matrix \hat{M}_k are obtained from (37) as

$$\bar{M}_k = E\{Z_k Z_k^T\} \tag{45}$$

$$\hat{M}_k = E\{\bar{M}_j\} = \frac{1}{B} \sum_{j=k-B+1}^k \bar{M}_j \tag{46}$$

Based on the IAE principle, the noise covariance \hat{Q}_k for the next time propagation is obtained combining the innovation covariance matrix \hat{M}_k and the Kalman gain K_k as

$$\hat{Q}_k = K_k \hat{M}_k K_k^T \tag{47}$$

In the previous section, it was shown that the noise covariances of GPS measurements are estimated independently of the adaptive KF. The adaptive KF explained in this section needs to estimate the covariance of process noise which is contributed only by inertial sensors. Thus, the roles of CSCF and KF are clearly divided in the proposed method, i.e., the adaptive CSCF estimates the covariances of GPS measurement noise and the adaptive KF estimates the covariances of inertial measurement noise.

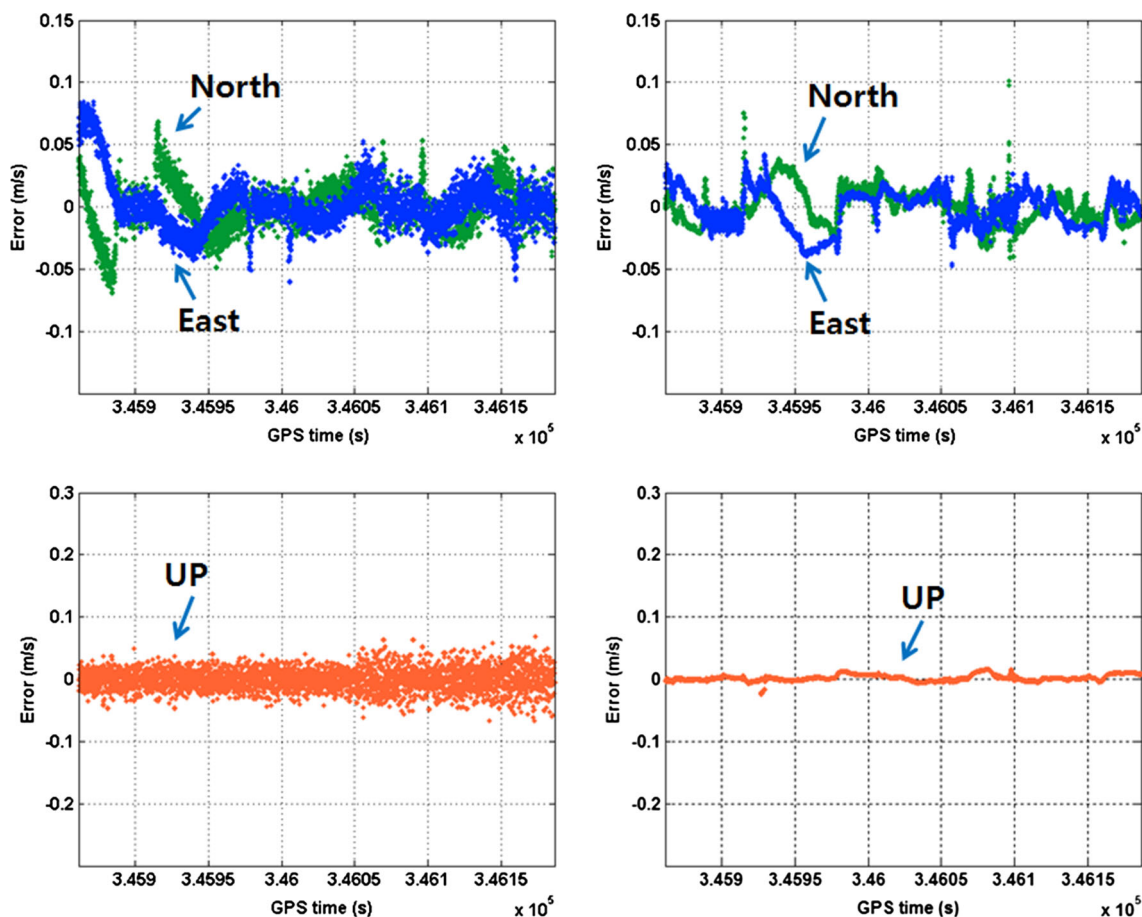


Fig. 6 Comparison of relative velocity error magnitudes with and without the proposed adaptive method

Simulation and experiment

A simulation and an experiment were performed to evaluate the feasibility of the proposed method. The simulation evaluates the accuracy improvement of the proposed method compared with the conventional method utilizing pre-defined noise covariances. The experiment evaluates the applicability of the proposed method in actual environment.

Simulation

For the simulation, a land vehicle simulator and a GPS/INS signal generator were utilized. The simulator generated the reference trajectory for a vehicle consisting of a tractor and a trailer. The simulation trajectory consists of two circular turns in opposite directions. Figure 5 shows the trajectory, the baseline between GPS antennas, and the relative velocity generated for the simulation. The signal generator generated GPS/INS measurements based on the reference trajectory.

To simulate two vehicles for relative navigation, a master (tractor) and a slave (trailer) running on the same trajectory at a speed of 80 km/h during 6 min were considered. It was assumed that each of the master and slave was equipped with a GPS receiver and an IMU. The stochastic errors of gyro and accelerometer were set as $0.0217^\circ/\sqrt{s}$ and $0.000723 \text{ (m/s)}/\sqrt{s}$, respectively. These parameters correspond to low-grade inertial sensors. The inertial sensor sampling rate was set as 100 Hz. The GPS pseudorange and carrier phase errors were modeled as the second-order Gauss-Markov process with the standard deviation of 23 m and 0.28 m/s, respectively. The GPS measurements were generated at 1 Hz. The lever arm was set as zero.

Figure 6 shows relative velocity errors in north, east, and vertical directions with or without the proposed adaptive method. As shown in the figure, the proposed adaptive method generated more accurate relative velocity estimates than the conventional method without adaptive filtering. It can be also seen that the accuracy in the vertical direction is improved much more than in the horizontal

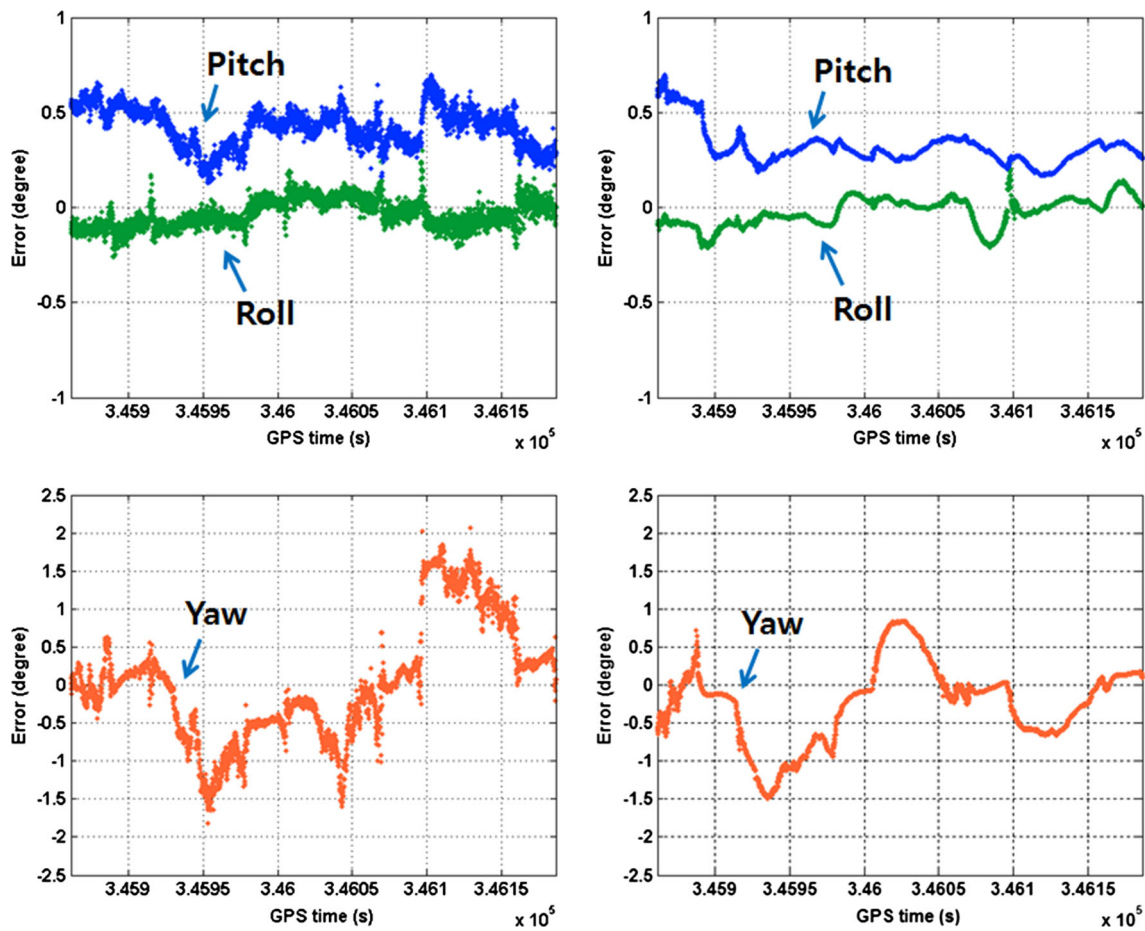


Fig. 7 Comparison of relative attitude error magnitudes with and without the proposed adaptive method

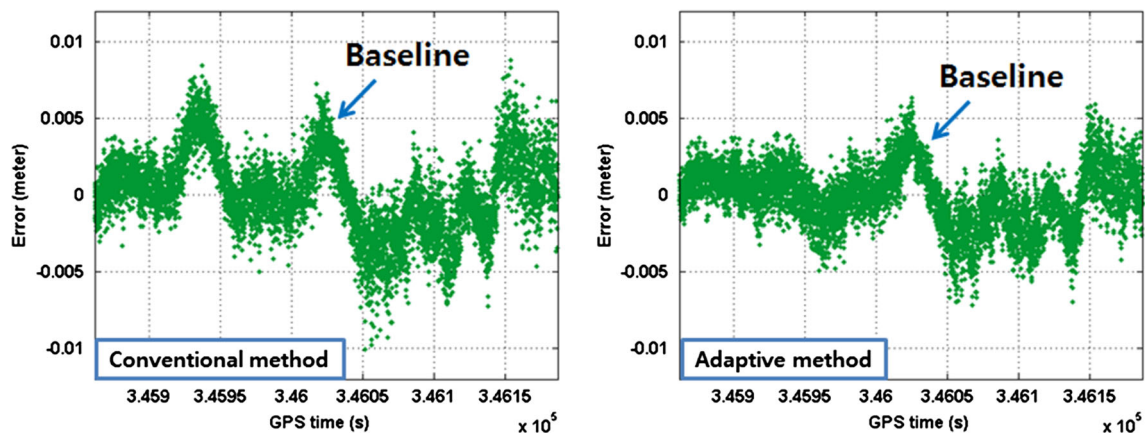


Fig. 8 Comparison of relative baseline error magnitudes with and without the proposed adaptive method

direction. The vertical errors are, in general, more influenced by incompletely modeled measurement errors than horizontal errors due to the intrinsic geometry characteristics between GPS satellites and receivers. This means that appropriately estimated measurement errors improve vertical accuracy more than horizontal accuracy. According to

the simulation results, the root-mean-square error (RMSE) of the relative velocity estimates by the proposed method in north, east, and vertical directions are 0.0138, 0.0155, and 0.0054 m/s, respectively.

Figures 7 and 8 show the error magnitudes of the relative attitude and baseline with or without the proposed

adaptive method. As shown in Fig. 7, yaw accuracy improves by the proposed method. The RMSE of the relative roll, pitch, and yaw by the proposed method are 0.0789° , 0.3326° , and 0.5786° , respectively. It can also be seen that the proposed method generates more accurate relative position estimates than the conventional method without adaptive filtering. The RMSE (3D) of the estimated baseline by the proposed method is 1.96 mm.

Field experiment

To evaluate the applicability of the proposed method in real environments, a kinematic experiment with two isolated ground vehicles was performed. The vehicles were stationary for 130 s at a static point and moved in cascaded formation around the trajectory shown in Fig. 9 for 200 s. Each of the front and rear vehicles was equipped with a

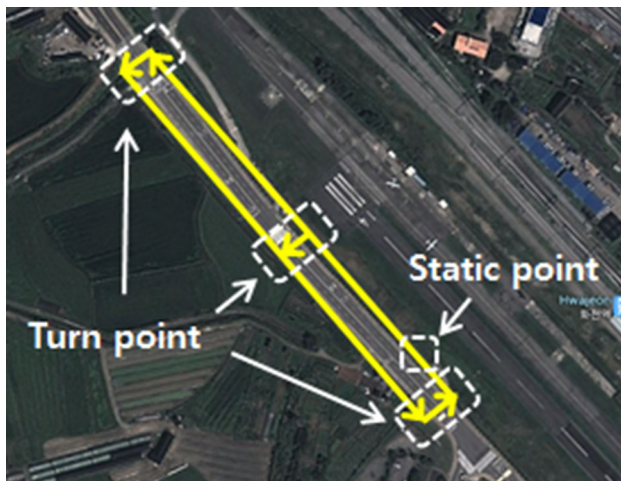


Fig. 9 Experiment environment and reference trajectory

Septentrio PolaRX2e GPS receiver and an MPU-6050 IMU. The noise specifications of the gyroscope and the accelerometer were $0.05^\circ/\text{s-rms}$ and $400 \mu\text{g}/\sqrt{\text{Hz}}$, respectively (InvenSense Inc. 2013). The sampling rate of inertial and GPS measurements was set as 20 and 1 Hz, respectively. The lever arm between the GPS antenna and the IMU was measured as 110.5 cm for the front vehicle and 210.5 cm for the rear vehicle. The GPS receiver provides dual-frequency measurements; however, only single-frequency measurements were utilized for relative GPS/INS. The field-collected dual-frequency measurements were processed to extract reference trajectory based on integer ambiguity resolutions. All the raw measurements were logged in the standard RINEX format.

Figure 10 shows the estimated standard deviations of carrier phase and pseudorange measurements. In the case of pseudorange measurements, standard deviations were estimated channel-by-channel. However, in the case of carrier phase measurements, a single standard deviation value was estimated and applied to all the channels since carrier phase errors are far less sensitive to signal environments than pseudorange errors. The areas marked by the rectangles in Fig. 10 correspond to the period when either an existing satellite disappears or a new satellite arises. In this case, the previously accumulated information for making innovation is not valid. For the reason, the noise variance was fixed until a sufficient number of measurements were obtained for an updated noise variance.

Figure 11 compares relative velocity errors and one-sigma envelopes, and Fig. 12 compares relative position errors and one-sigma envelopes. The estimation errors were computed by the differences between the solutions generated by the proposed method and the references generated by dual-frequency RTK method. It should be noted that if the covariances were estimated incorrectly,

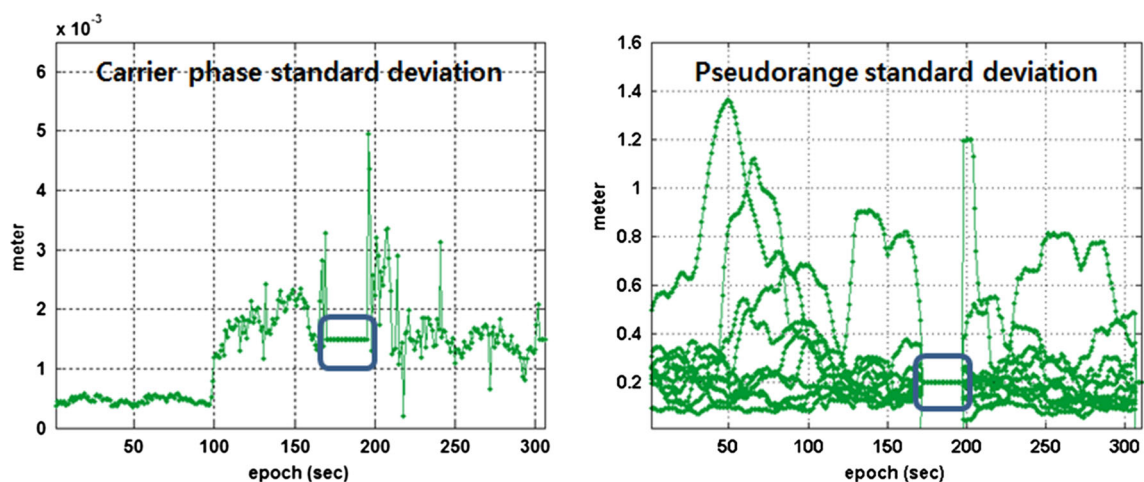


Fig. 10 Estimated standard deviations of carrier phase and pseudorange measurements

inconsistency between the one-sigma envelopes and the estimation error would be noticeable. The estimation error would be much larger than the magnitude indicated by the one-sigma envelopes even after the filter enters into the steady state (Lee et al. 2013). However, it can be seen in

Figs. 11 and 12 that the one-sigma envelopes constrain the actual estimation errors reasonably and inconsistency does not occur when the proposed adaptive method is utilized. This result shows that the proposed method estimates the covariance appropriately in actual environment. The

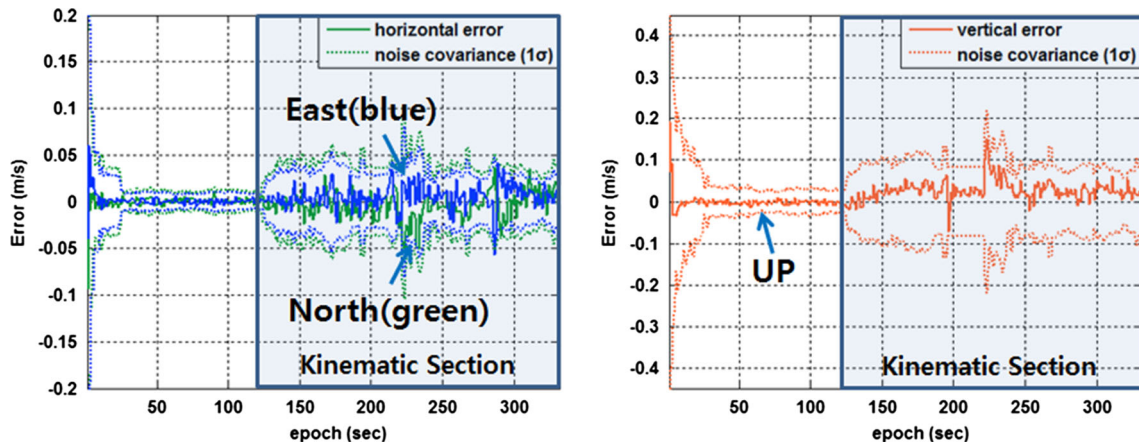


Fig. 11 Comparison of relative velocity errors (solid lines) and their one-sigma envelopes (dotted lines)

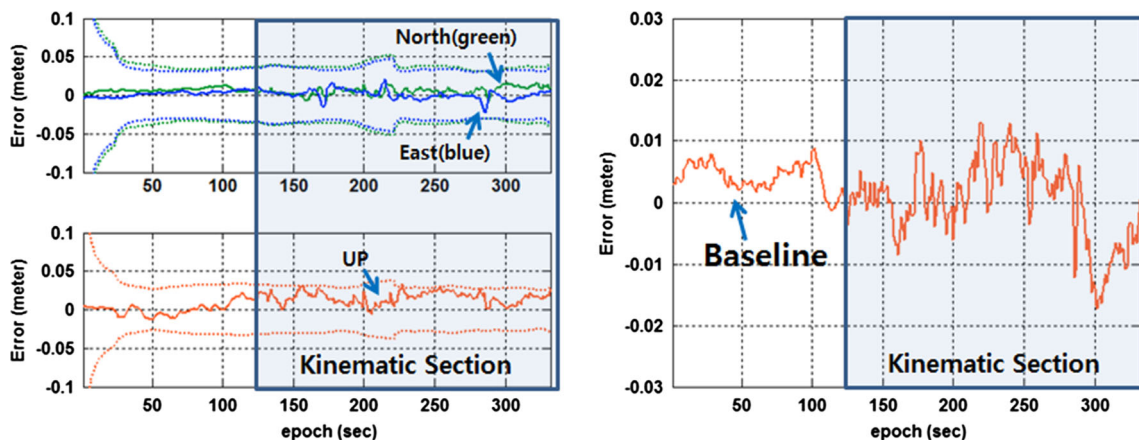


Fig. 12 Comparison of relative position errors (solid lines) and their one-sigma envelopes (dotted lines)

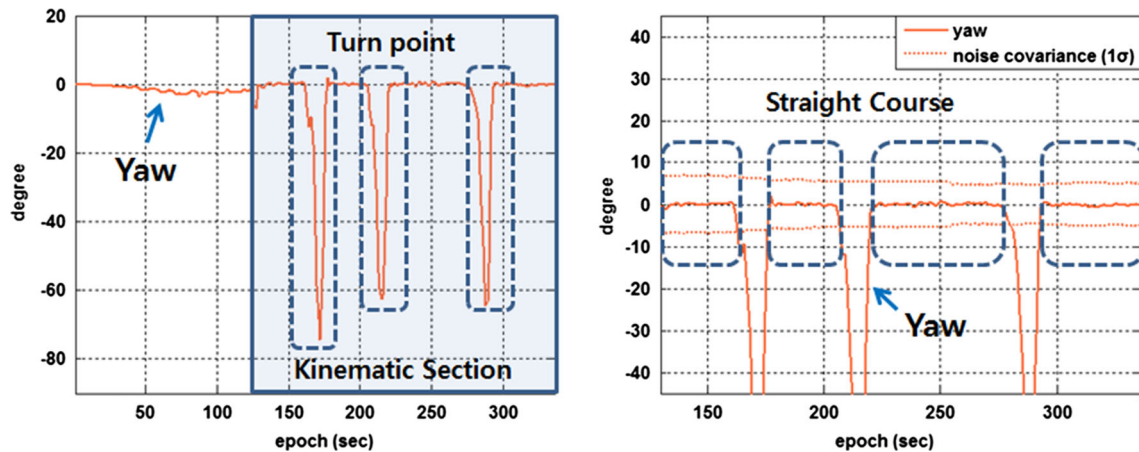


Fig. 13 Comparison of relative yaw (solid line) and one-sigma envelopes (dotted lines)

RMSE of the relative positions in north, east, and vertical directions were 0.0074, 0.0055, and 0.0147 m, respectively, with respect to the reference RTK solutions. The RMSE of the baseline was 0.0059 m. The RMSE of the relative velocity in north, east, and vertical directions were 0.0130, 0.0121, and 0.0315 m/s, respectively.

Figure 13 shows the relative yaw and its one-sigma envelopes generated by the proposed method. Since the dual-frequency GPS measurements cannot provide reference attitude information by the RTK processing, it is difficult to obtain relative yaw errors. However, the relative yaw between the two vehicles would be practically zero when the two vehicles move along the same straight road lane. For the reason, the relative yaw can be considered as the relative yaw error during the straight movements. In the right plot of Fig. 13, four areas marked by dashed rectangles correspond to the periods during which the two vehicles are in straight movement so that the relative yaw equals the relative yaw error. In the four areas, it can be seen that the relative yaw errors are well within the one-sigma envelopes. Thus, it can also be considered that relative yaw is appropriately estimated.

Conclusions

An efficient GPS/INS integration method was proposed for adaptive relative navigation. The proposed method avoids the cascaded filtering problem by two fundamentally different filters, i.e., the adaptive SD PD CSCF and the adaptive velocity-aided GPS/INS KF. The adaptive SD PD CSCF generates GPS position with the noise covariance estimates of carrier phase and pseudorange measurements. The adaptive KF generates accurate relative velocity and attitude information at high output rate with the noise covariance estimates of the inertial sensors. By simulation and experiment results, it was shown that the proposed method improves accuracy of navigation solution by appropriate noise covariance estimation. For further improvement, covariance estimation techniques for multi-constellation global navigation satellite systems (GNSS) need to be developed with more field experiments.

Acknowledgments This research was supported by a grant from National Agenda Project (NAP) funded by Korea Research Council of Fundamental Science and Technology.

References

Almagbile A, Wang J, Ding W (2010) Evaluating the performances of adaptive Kalman filter methods in GPS/INS integration. *J Glob Position Syst* 9(1):33–40

- Alonso R, Crassidis JL, Junkins JL (2000) Vision-based relative navigation for formation flying of spacecraft. In: AIAA guidance, navigation, and control conference and exhibit, Denver, CO
- Baek K, Bang H (2013) Adaptive sparse grid quadrature filter for spacecraft relative navigation. *Acta Astronaut* 87:96–106
- Bever G, Urschel P, Hanson CE (2002) Comparison of relative navigation solutions applied between two aircraft. NASA TM-2002-210728
- Chu L, Shi Y, Zhang Y, Liu H, Xu M (2010) Vehicle lateral and longitudinal velocity estimation based on adaptive Kalman filter. *IEEE Int Conf Adv Comput Theory Eng* 3:V3-325
- Dar K, Bakhouya M, Gaber J, Wack M, Lorenz P (2010) Wireless communication technologies for ITS applications [topics in automotive networking]. *Commun Mag IEEE* 48(5):156–162
- Ding W, Wang J, Rizos C, Kinlyside D (2007) Improving adaptive Kalman estimation in GPS/INS integration. *J Navig* 60(3):517
- Ding W, Wang J, Li Y, Mumford P, Rizos C (2008) Time synchronization error and calibration in integrated GPS/INS systems. *ETRI J* 30(1):59–67
- Fakharian A, Gustafsson T, Mehrfam M (2011) Adaptive Kalman filtering based navigation: an IMU/GPS integration approach. In: IEEE international conference on networking, sensing and control, pp 181–185
- Fosbury AM, Crassidis JL (2006) Kalman filtering for relative inertial navigation of uninhabited air vehicles. In: AIAA guidance, navigation, and control conference and exhibit, pp 21–24
- Garcia-Velo J (1997) Determination of noise covariances for extended Kalman filter parameter estimators to account for modeling errors. Ph.D. thesis, University of Cincinnati
- Gerla M, Kleinrock L (2011) Vehicular networks and the future of the mobile internet. *Comput Netw* 55(2):457–469
- Groves PD (2008) Principles of GNSS, inertial, and multisensor integrated navigation systems. Artech House, London
- Hanlon PD, Maybeck PS (2000) Multiple-model adaptive estimation using a residual correlation Kalman filter bank. *IEEE Trans Aerosp Electron Syst* 36(2):393–406
- Hao Y, Guo Z, Sun F, Gao W (2009) Adaptive extended Kalman filtering for SINS/GPS integrated navigation systems. In: IEEE international joint conference on computational sciences and optimization, pp 192–194
- Hatch R (1983) The synergism of GPS code and carrier measurements. In: Proceeding of the international geodetic symposium on satellite doppler positioning, pp 1213–1231
- InvenSense Inc (2013) MPU-6000 and MPU-6050 product specification revision 3.4. <http://invensense.com/mems/gyro/documents/PS-MPU-6000A-00v3.4.pdf>
- Kailath T (1971) A note on least-squares estimation by the innovations method. *IEEE Conf Decis Control* 10:407–411
- Kaplan ED, Hegarty CJ (2006) Understanding GPS: principles and applications. Artech House, London
- Lee HK, Rizos C (2008) Position-domain hatch filter for kinematic differential GPS/GNSS. *IEEE Trans Aerosp Electron Syst* 44(1):30–40
- Lee HK, Lee JG, Roh YK, Park CG (1998) Modeling quaternion errors in SDINS: computer frame approach. *IEEE Trans Aerosp Electron Syst* 34(1):289–300
- Lee HK, Lee JG, Jee GI (2002) Calibration of measurement delay in GPS/SDINS hybrid navigation. *AIAA J Guid Control Dyn* 25(2):240–247
- Lee HK, Rizos C, Jee GI (2005) Position domain filtering and range domain filtering for carrier-smoothed-code DGNSS: an analytical comparison. *IEE Proc Radar Sonar Navig* 152(4):271–276
- Lee JY, Kim HS, Choi KH, Park JD, Kim MW, Lee HK (2011) A study of covariance estimation to apply carrier-smoothed-code

- filter in GNSS. In: Proceeding of the international science and technology conference, pp 7–9
- Lee JY, Kim HS, Choi KH, Cho JH, Lee HK (2013) Adaptive position-domain carrier-smoothed code filter based on innovation sequences. *Radar Sonar Navig IET* 8(4):336–343
- Li W, Wang J (2013) Effective adaptive Kalman filter for MEMS-IMU/magnetometers integrated attitude and heading reference systems. *J Navig* 1(1):1–15
- Li B, Rizos C, Lee HK, Lee HK (2006) A GPS-slaved time synchronization system for hybrid navigation. *GPS Solut* 10(3):207–217
- Li W, Gong D, Liu M, Chen JA, Duan D (2013) Adaptive robust Kalman filter for relative navigation using global position system. *Radar Sonar Navig IET* 7(5):471–479
- Magill D (1965) Optimal adaptive estimation of sampled stochastic processes. *IEEE Trans Autom Control* 10(4):434–439
- Maybeck P (1989) Moving-bank multiple model adaptive estimation and control algorithms: an evaluation. *Control Dyn Syst* 31:1–31
- Mehra R (1970) On the identification of variances and adaptive Kalman filtering. *IEEE Trans Autom Control* 15(2):175–184
- Mehra R (1971) On-line identification of linear dynamic systems with applications to Kalman filtering. *IEEE Trans Autom Control* 16(1):12–21
- Mohamed AH, Schwarz KP (1999) Adaptive Kalman filtering for INS/GPS. *J Geodesy* 73(4):193–203
- Nilsson JO, Handel P (2010) Time synchronization and temporal ordering of asynchronous sensor measurements of a multi-sensor navigation system. In: *IEEE/ION position location and navigation symposium (PLANS)*, pp 897–902
- Park JD, Kim MW, Lee JY, Kim HS, Lee HK (2011) An integration method for L1 GPS receiver and MEMS IMU based on dual filters. In: *International science and technology conference*, pp 51–56
- Yun X, Bachmann ER, McGhee RB et al (1999) Testing and evaluation of an integrated GPS/INS system for small AUV navigation. *IEEE J Oceanic Eng* 24(3):396–404
- Zhou W, Qiao XW, Meng F, Zhang H (2010) Study on SINS/GPS tightly integrated navigation based on adaptive extended Kalman filter. In: *IEEE international conference on information and automation*, pp 2344–2347
- Je Young Lee** is a Ph.D. candidate at School of Electronics, Telecommunication and Computer Engineering, Korea Aerospace University. His research interests include fault detection, adaptive filtering, INS and its applications.
- Hee Sung Kim** was a Ph.D. candidate at School of Electronics, Telecommunication and Computer Engineering, Korea Aerospace University at this manuscript submission. He received Ph.D. degree in 2014 and is now at Korea Aerospace Research Institute (KARI). His research interests include long-baseline integer ambiguity resolution and Network RTK system design.
- Kwang Ho Choi** is a Ph.D. candidate in School of Electronics, Telecommunication and Computer Engineering, Korea Aerospace University. His research interests include network-based real-time high-resolution TEC map generation and GPS/INS integration.
- Joonhoo Lim** is a Ph.D. candidate in School of Electronics, Telecommunication and Computer Engineering, Korea Aerospace University. He received the certification of the Wipro-KRCF project team. He worked as a researcher at Korea Aerospace Research Institute. His research interests include hybrid positioning system and integrity analysis.
- Sebum Chun** is a senior researcher in Korea Aerospace Research Institute (KARI). He received Ph.D. degree from Department of Aerospace Engineering of Konkuk University in 2008. His research interests include inertial and satellite navigation systems.
- Hyung Keun Lee** is a Professor at School of Electronics, Telecommunication and Computer Engineering, Korea Aerospace University. He received Ph.D. degree from the School of Electrical Engineering and Computer Science, Seoul National University in 2002. His research interests include PNT systems, navigation networks, and avionics.